GREENER AVIATION
OCTOBER 11th TO 13th 2016

FAN WAKE MODELLING FOR COMPUTATIONAL AEROACOUSTIC SIMULATIONS OF TURBULENCE-CASCADE INTERACTION NOISE

Fernando Gea-Aguilera(1), James Gill(2), Xin Zhang(3), Thomas Nodé-Langlois(4)

(1)(2) Airbus Noise Technology Centre, University of Southampton, Southampton, SO16 7QF, UK.
(1)Email: f.gea-aguilera@soton.ac.uk
(3) The Hong Kong University of Science and Technology, Hong Kong SAR, China.
(4) Airbus Operations S.A.S., 31060 Toulouse, France.

KEYWORDS: computational aeroacoustics, synthetic turbulence, turbulence-cascade interaction noise

ABSTRACT:

The present work addresses the numerical modelling of fan wakes using synthetic turbulence and its influence on turbulence-cascade interaction noise predictions. Initial results show that cascade noise only depends on the circumferentially-averaged turbulence spectra that interact with the cascade. Consequently, isotropic turbulence produces noise predictions with approximately the same level of accuracy than fan wakes with cyclostationary variations in both turbulent kinetic energy and integral length scale. The paper also includes a parameter study on the effects of vane count and camber on cascade noise from thick aerofoils. Numerical results show that vane count may have a significant effect on noise predictions at low frequencies, whereas the effects of camber are negligible.

1. INTRODUCTION

Stringent regulations on noise emissions have recently been set in Europe to ensure a sustainable development of commercial aviation [1]. Today, broadband noise from aircraft engines is a major contributor to the overall noise level, which is mainly caused by the interaction of the fan wakes with the Outlet Guide Vanes (OGVs) [2], as shown in Fig. 1. The aim of the current work is to improve understanding of engine fan broadband noise.

Recently, promising broadband noise predictions have been obtained by using a Lattice-Boltzmann solver to investigate complex fan-OGV configurations [3, 4]. Other numerical studies have performed Large Eddy Simulations (LES) of the OGV stage [5]. Such approaches aim at reproducing realistic experimental or inflight conditions, which make it difficult to isolate different sources of noise and to assess the influence of classic modelling assumptions, such as frozen turbulence, isotropic/anisotropic turbulence in the fan wakes, and steady/unsteady mean flows, among others. Alternatively, fundamental numerical works that solve simplified governing equations, such as the full or Linearised Euler Equations (LEEs), can be used to assess the effects of certain modelling assumptions and design parameters on broadband noise predictions.

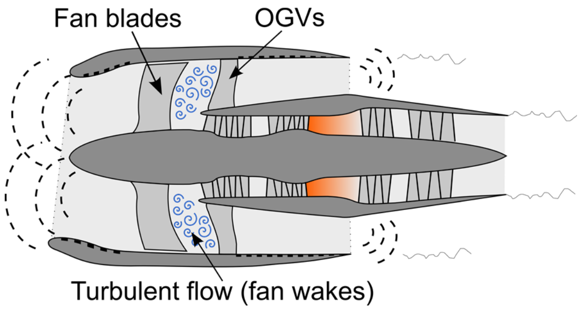

Figure 1. Schematic of engine fan broadband noise due to fan wake-OGV interaction

In this work, two-dimensional Computational AeroAcoustic (CAA) simulations are performed to study simplified but representative configurations of fan wake-OGV interaction noise. A synthetic turbulence method that is based on digital filters is used in a LEE solver to reproduce the statistics of the fan wakes. A number of assumptions are investigated to model the turbulent flow in the fan wakes, such as homogeneous isotropic turbulence, and non-homogeneous turbulence with spatio-temporal variations in intensity and integral length scale. Synthetic turbulence with the correct statistics of the fan wakes is injected into the CAA domain to model the interaction with a cascade, which radiates broadband noise upstream and downstream of the cascade. The present work constitutes an extension of a previous investigation into the effects of aerofoil geometry on isotropic turbulence-cascade interaction noise [6].

This paper is organised as follows. Section 2 summarises previous works in the field of CAA simulations of turbulence-cascade interaction noise. The CAA solver that is used in the current work is presented in Section 3. In Section 4, an advanced digital filter method is adapted to generate synthetic turbulence with the desired fan wake statistics. The influence of fan wake modelling assumptions on cascade noise is assessed in Section 5. Finally, the effects of vane count and aerofoil camber are investigated in Section 6.

2. PREVIOUS WORK

Initial numerical studies in the field of turbulence-cascade interaction noise focused on modelling the interaction of single frequency gusts with aerofoil cascades [7, 8]. For instance, Envia [7] investigated the interaction of three harmonic gusts with a quasi two-dimensional cascade with realistic OGV geometries. Recently, Paruchuri *et al*. [9] investigated the effects of vane geometry in two-dimensional simulations using a harmonic vortical gust decomposition in a linearised Navier-Stokes equation solver. A parameter study performed at a fixed reduced frequency, $fc/U = 1.88$ where c is the aerofoil chord and U is the upstream mean flow velocity, showed small effects ($\sim 1 - 2\ \mathrm{dB}$) on overall noise levels caused by aerofoil thickness, camber, angle of attack, and swirl in the mean flow.

Several harmonic gusts, whose amplitudes are proportional to a specified velocity spectrum, can be superimposed to produce synthetic turbulence with the key features of the fan wakes. This type of synthetic turbulence is often referred to as a summation of Fourier modes. In this context, Polacsek *et al.* [10] performed three-dimensional CAA simulations of a single flat plate OGV passage with isotropic turbulence that only included the upwash fluctuating velocity component.

Digital filter methods generate stochastic velocity fields by filtering random data, such as white noise signals. Based on the Random Particle-Mesh (RPM) method [11], Dieste (Chapter 6 in [12]) generated two-dimensional fan wakes with spatio-temporal variations in the turbulent kinetic energy, so that the resulting turbulent flow was non-homogeneous and non-stationary. Assuming a constant integral length scale, Λ, and using the cyclostationary analysis of Jurdic *et al.* [13] to define the half-wake width, $L_w = \Lambda/0.42$, Dieste [12] showed that an increase in the separation between fan wakes that interact with a single flat plate scales down the noise levels, but maintains the shape of the noise spectra.

Using a similar description of the fan wakes as in Dieste's work [12], Wohlbrandt *et al.* [14] reported unaffected cascade noise when increasing the rotation speed of the fan wakes that interact with a two-dimensional cascade of cambered aerofoils. Additionally, Wohlbrandt *et al.* [14] included cyclostationary variations in the integral length scale of the fan wakes, although their effect on noise spectra predictions was inconclusive.

Gea-Aguilera *et al.* [6] performed a CAA study on isotropic turbulence-cascade interaction noise, showing that the effect of aerofoil thickness is to reduce noise levels at sufficiently high frequencies, as occurs in single aerofoils (for instance, see [15, 16]. Variations in stagger angle and gap-to-chord ratio induced a change in the peaks and valleys of the noise spectra, but the overall noise level remained approximately the same. Gea-Aguilera *et al.* [6] also modelled spatio-temporal variations in the turbulence kinetic energy with a uniform integral length scale to reproduce the fan wakes, and suggested that sound power spectra scale with the circumferentially-averaged mean square turbulent velocity. This finding was also highlighted in the analytical model of Ju *et al.* [17], and is consistent with the results reported by Dieste [12] and Wohlbrandt [14].

3. CAA SOLVER

In the current work, the LEEs are solved in the time domain with the mean flow density and speed of sound set to $\rho_0 = 1.2\ \mathrm{Kg/m^3}$ and $c_0 = 340\ \mathrm{m/s}$, respectively. The characteristics of the CAA solver are detailed in prior leading edge noise studies [18, 19]. The reference value to compute sound PoWer Level (PWL) spectra is $10^{-12}\ \mathrm{W}$. All numerical simulations presented in this work used the IRIDIS 4 high performance computing facility at the University of Southampton.

4. NUMERICAL FAN WAKE MODELLING

In this section, three different modelling strategies are presented to reproduce the turbulence statistics of the fan wakes:

- Isotropic turbulence with constant turbulence intensity and integral length scale.
- Cyclostationary variations in turbulent kinetic energy with constant integral length scale.
- Cyclostationary variations in both turbulent kinetic energy and integral length scale.

A cyclostationary analysis can be performed when periodic variations in time are assumed for the fan wake statistics [13]. Although the present study is restricted to two-dimensional simulations to reduce the computational cost, the modelling strategies presented herein can be extended to fully three-dimensional simulations.

4.1 Isotropic turbulence

The advanced digital filter method proposed by Gea-Aguilera *et al.* [18], which is based on the RPM method [11] and synthetic eddy methods [20, 21], is used herein to generate isotropic synthetic turbulence with the spectral content of the two-dimensional von Kármán spectrum defined as

$$E^{(2D)}(k) = \frac{110 u_{rms}^2 \Lambda}{27\pi} \frac{(k/k_e)^4}{[1+(k/k_e)^2]^{17/6}}, \qquad (1)$$

where u_{rms} is the root-mean-square fluctuating velocity, k is the overall wavenumber, and $k_e = [\sqrt{\pi}\Gamma(5/6)]/[\Lambda\Gamma(1/3)]$ with $\Gamma()$ as the Gamma function.

The resulting turbulent flow is obtained by introducing a number of synthetic eddies into the CAA domain through an injection plane, as is shown in Fig. 2. Unlike in previous CAA studies on fan wake modelling [12, 14], the injection plane extends all along the circumferential direction, i.e., from the top edge of the CAA domain to the bottom edge, where periodic boundary conditions are used. This avoids the use of further assumptions in cascade noise simulations, such as considering that the vanes are uncorrelated noise sources [14].

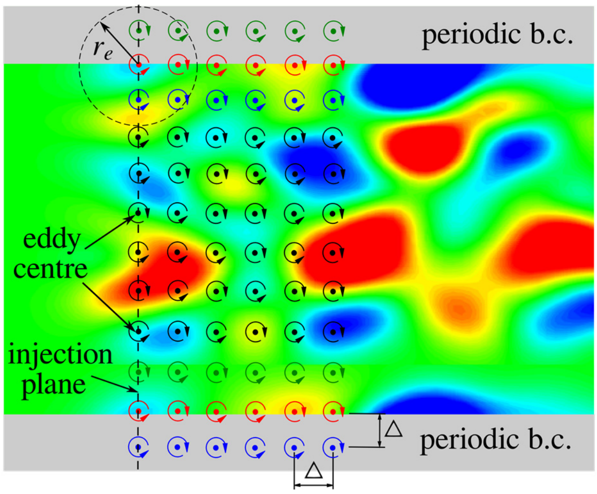

Figure 2. Injection plane of synthetic turbulence and input parameters r_e and Δ

Each eddy is obtained from a summation of Gaussian eddies, which defines a new eddy profile that can match a target energy spectrum. The fluctuating velocity field introduced by each eddy is divergence-free and takes the form

$$u_x(\mathbf{x}) = -\epsilon\Delta \sum_{i=1}^{N_e} \frac{\sqrt{2\pi u_{rms,i}^2}}{\Lambda_i^2} (y - y_e) \exp\left(-\frac{\pi r^2}{2\Lambda_i^2}\right), \qquad (2)$$

$$u_y(\mathbf{x}) = \epsilon\Delta \sum_{i=1}^{N_e} \frac{\sqrt{2\pi u_{rms,i}^2}}{\Lambda_i^2} (x - x_e) \exp\left(-\frac{\pi r^2}{2\Lambda_i^2}\right), \qquad (3)$$

where $\mathbf{x} = (x, y)$ is a point in the source region, (x_e, y_e) corresponds to the eddy centre, $\epsilon = \pm 1$ is a random number that defines the direction of rotation of the eddy, Δ is the eddy spacing, and r is the distance from a point in the source region to the eddy centre. In order to recover the correct statistics of the turbulent flow, Gea-Aguilera *et al.* [18] showed that the eddy spacing and the eddy radius should satisfy $\Delta \leq \min\{\Lambda_i\}/2$ and $r_e \geq 3\max\{\Lambda_i\}/2$, respectively, for $i = 1, \ldots, N_e$. Once the eddies are injected into the CAA domain, they are convected as frozen turbulence by the mean flow. It should be noted that the frozen turbulence assumption has been shown to be accurate in practical cases of turbulence-aerofoil interaction noise [12].

4.2 Variations in turbulence intensity

Previous analytical and numerical studies have proposed to split the turbulence downstream of the fan stage into background and wake turbulence [12, 17, 22].

- Background turbulence flow is typically modelled by a constant turbulent kinetic intensity and integral length scale.
- The fan wakes include spatio-temporal variations in the turbulent kinetic energy, but the integral length scale also takes a constant value.

Due to the absence of accurate information, and to simplify the analysis, the integral length scales in the background and wake turbulence are often assumed to be the same [12, 22]. However, Ju *et al*. [17] showed non-negligible variations in the shape of the noise spectra when using different integral length scales for background and wake turbulence.

In this section, the background turbulent flow is neglected, and the fan wakes are generated by assuming cyclostationary variations in the turbulent kinetic energy, following a similar approach as in Dieste's work [12]. To this end, the amplitude of the synthetic eddies defined by Eqs. 2 and 3 is modulated by a train of Gaussian functions,

$$A_w(y_e,t) = \sum_{i=-\infty}^{+\infty}\left\{\exp\left[-\frac{\ln 2}{h_w^2}(y_e-\Omega R(t+iT_w))^2\right]\right\}^{\frac{1}{2}} \quad (4)$$

where t is the time, h_w is the semi-wake width, Ω is the angular speed of the fan wakes, R is the radius of the wrapped CAA domain, and $T_w = 2\pi/(n_w\Omega)$ is the period of the fan wakes, with n_w being the number of wakes included in the CAA domain. Although the fan wakes usually present a certain degree of skewness, and are not perfectly symmetric, Gaussian functions are considered a good approximation for the distribution of the turbulent kinetic energy in the fan wakes [22]. Due to the frozen turbulence assumption, the current CAA methodology cannot account for the wake spreading and increased overlapping that occurs as the fan wakes are convected downstream of the fan stage.

4.3 Variations in turbulence intensity and integral length scale

To date, few works have studied the distribution of the integral length scale within a fan wake [14, 23]. In this work, circumferential variations in the integral length scale are modelled by

$$\Lambda_w(y_e,t) = \Lambda_{min} + (\Lambda_{max}-\Lambda_{min})\left[1-\frac{A_w(y_e,t)-\min\{A_w(y_e,t)\}}{\max\{A_w(y_e,t)\}-\min\{A_w(y_e,t)\}}\right], \quad (5)$$

where the minimum integral length scale, Λ_{min}, is found at the peak of turbulent kinetic energy in the fan wakes, following similar trends to those presented by Wohlbrandt *et al*. [14] in a Unsteady Reynolds-Averaged Navier-Stokes (URANS) simulation of fan blades. In order to account for spatio-temporal variations in both the turbulent kinetic energy and integral length scale, Eqs. 2 and 3 are modified as follows

$$u_x(\mathbf{x}) = -\epsilon\Delta A_w \sum_{i=1}^{N_e}\frac{\sqrt{2\pi u_{rms,i}^2}}{\Lambda_i^2\frac{\Lambda_w^2}{\Lambda_{max}^2}}(y-y_e)\exp\left(\frac{-\pi r^2}{2\Lambda_i^2\frac{\Lambda_w^2}{\Lambda_{max}^2}}\right), \quad (6)$$

$$u_y(\mathbf{x}) = \epsilon\Delta A_w \sum_{i=1}^{N_e}\frac{\sqrt{2\pi u_{rms,i}^2}}{\Lambda_i^2\frac{\Lambda_w^2}{\Lambda_{max}^2}}(x-x_e)\exp\left(\frac{-\pi r^2}{2\Lambda_i^2\frac{\Lambda_w^2}{\Lambda_{max}^2}}\right). \quad (7)$$

It should be mentioned that a different integral length scale distribution was found by Maunus *et al*. [23] in Computational Fluid Dynamic (CFD) computations of a fan stage. Since the present technique is not restricted to the turbulence intensity and integral length scale variations defined by Eqs. 4 and 5, alternative distributions could potentially be tested.

4.4 Validation of numerical implementation

Although the spectral content of the fan wakes has been reported to closely follow a von Kármán spectrum in experiments [2], Gaussian spectra have been used to generate synthetic turbulence as a simplified approach to the spectral content in the fan wakes [12, 14].

Both Gaussian and von Kármán spectra are used herein to generate synthetic turbulence with the statistics of the fan wakes using the modelling assumptions presented in Sections 4.1, 4.2, and 4.3.

4.4.1 Gaussian spectrum

In this section, isotropic synthetic turbulence is generated to follow the two-dimensional Gaussian spectrum as defined by Kraichnan [24],

$$E^{(2D)}(k) = \frac{2u_{rms}^2\Lambda^4 k^3}{\pi^2}\exp\left(-\frac{\pi r^2}{2\Lambda^2}\right), \quad (8)$$

where $T_u = u_{rms}/U_x = 0.017$, $\Lambda = 0.008$ m and the mean flow Mach number is set to $M_x = 0.3$.

In order to model variations in the turbulence intensity using Eq. 4, the semi-wake width is given by $h_w = \Lambda/0.42$ according to Jurdic *et al.* [13]. A total number of $n_w = 2$ wakes are injected into the CAA domain. To simplify the post-processing of the fan wake statistics, the rotational speed is set to zero ($\Omega = 0$ rad/s), so that turbulence is homogeneous in the x-direction.

Variations in the integral length scale using Eq. 5 are performed by setting $\Lambda_{min} = 0.004$ m and $\Lambda_{max} = 4\Lambda_{min}$.

For validation purposes, synthetic turbulence is injected into an empty CAA domain with uniform grid spacing 1.1×10^{-3} m, whose dimensions are $x \in [-0.096, 0.16]$ and $y \in [-0.125, 0.125]$ in m. Fig. 3 shows the CAA domain for the validation case with cyclostationary variations in the turbulence intensity. All simulations were run for 4.8×10^6 iterations using a non-dimensional time step, $\mathrm{d}tc_0/L_{ref}$ with $L_{ref} = 1$ m, of 5×10^{-4}. Velocity samples were collected at 100 monitor points uniformly distributed along the circumferential direction, y, downstream of the inlet section.

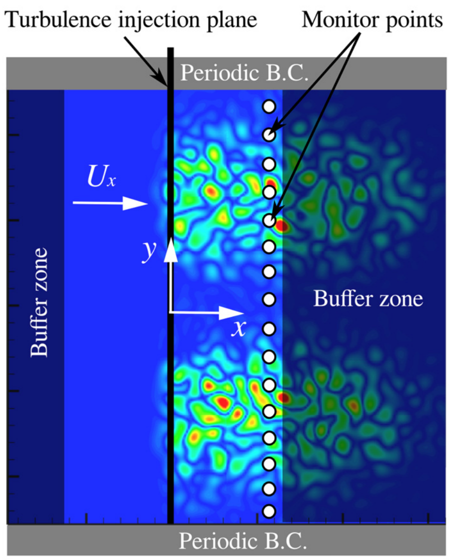

Figure 3. CAA domain for validation of fan wake statistics and contours of fluctuating vorticity magnitude assuming $\boldsymbol{T_u(y)}$, and $\boldsymbol{\Lambda} = \mathbf{const}$.

Fig. 4 shows variations in $\|\boldsymbol{u}\|_{rms} = \sqrt{u_{x,rms}^2 + u_{y,rms}^2}$ for the different fan wake modelling approaches. A good agreement is found between analytical and numerical results, giving validation to the numerical fan wake injection method.

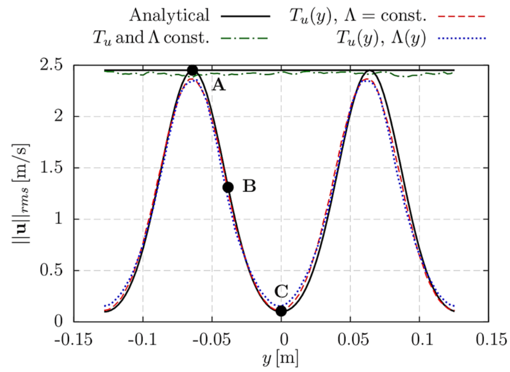

Figure 4. Circumferential distribution of root-mean-square fluctuating velocity magnitude for different fan wake modelling assumptions

One-dimensional spectra are defined in [25] as

$$E_{ij}^{(2D)}(k_x) = 2\int_{-\infty}^{\infty} \Phi_{ij}^{(2D)}(k_x, k_y)\mathrm{d}k_y, \tag{9}$$

where $\Phi_{ij}^{(2D)}(k_x, k_y)$ is the velocity spectrum that can be obtained from the Fourier transform of the velocity correlation tensor. Fig. 5 shows analytical and numerical one-dimensional spectra averaged in the circumferential direction, where an agreement of better than 1 dB is found at all frequencies.

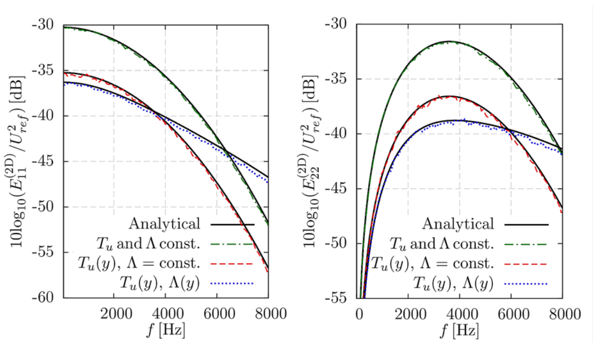

Figure 5. Gaussian one-dimensional spectrum of streamwise (left) and transverse (right) fluctuating velocity averaged in the circumferential direction

The integral length scale distribution can be obtained from to streamwise one-dimensional spectra [25] by using

$$\Lambda = \lim_{f \to 0} \frac{U_x E_{11}(f)}{4u_{x,rms}^2}. \tag{10}$$

Taking advantage of the flatness of $E_{11}(f)$ at low frequencies, the value of $E_{11}(f=0)$ can be approximated by taking the averaged value of the spectrum for $f < 250\ \mathrm{Hz}$. This strategy is similar to that used by Ganz *et al.* [2] to compute the integral length scale from experimental hotwire measurements of fan wakes. Fig. 6 shows the circumferential distribution of the integral length scale, in which a good agreement is observed.

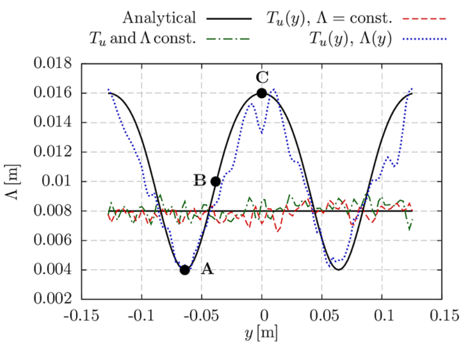

Figure 6. Circumferential distribution of integral length scale for different fan wake modelling assumptions

4.4.2 Von Kármán spectrum

Following a similar methodology as described in Section 4.4.1, the numerical implementation is also validated for the von Kármán spectrum, as defined in Eq. 1 with $T_u = 0.017$, $\Lambda = 0.008\ \mathrm{m}$ and the mean flow Mach number is set to $M_x = 0.3$. Since the von Kármán spectrum presents a broader spectral content than a Gaussian spectrum, the CAA mesh has been refined to ensure that the small vortical structures are convected without dissipation. Thus, the grid spacing is now set to $2.1 \times 10^{-4}\ \mathrm{m}$.

The isotropic turbulence is recovered from a superposition of $N_e = 5$ Gaussian eddies in Eqs. 2 and 3 with the values that are given in Tab. 1.

The amplitude of the isotropic turbulent flow is modulated by using Eq. 4 with the same input parameters as specified in Section 4.4.1. In order to include variations in the integral length scale between $\Lambda_{min} = 0.004\ \mathrm{m}$ and $\Lambda_{max} = 4\Lambda_{min}$, Eqs. 6 and 7 are used with the values given in Tab. 2.

Λ_i [m]	$u^2_{rms,i}$ [m/s]
2.524×10^{-2}	5.194×10^{-2}
1.401×10^{-2}	2.152×10^{-1}
7.285×10^{-3}	3.012×10^{-1}
3.023×10^{-3}	4.667×10^{-1}
2.238×10^{-3}	8.929×10^{-3}

Table 1. Parameters for Gaussian superposition to produce von Kármán spectrum with $T_u = 0.017$, and $\Lambda = 0.008\ \mathrm{m}$ at $M_x = 0.3$

Λ_i [m]	$u^2_{rms,i}$ [m/s]
5.048×10^{-2}	5.176×10^{-2}
2.801×10^{-2}	2.180×10^{-1}
1.457×10^{-2}	2.759×10^{-1}
7.117×10^{-3}	2.522×10^{-1}
2.801×10^{-3}	3.721×10^{-1}

Table 2. Parameters for Gaussian superposition to produce von Kármán spectrum with $T_u = 0.017$, and $\Lambda = 0.016\ \mathrm{m}$ at $M_x = 0.3$

Fig. 7 shows fluctuating vorticity magnitude using different fan wake modelling assumptions. When comparing Figs. 7(a) and 7(b), an amplitude decay can be observed from the fan wake centreline in the case with variations in the turbulence intensity. However, the size of the turbulent structures remains the same throughout the domain. In contrast, Fig. 7(c) shows significant variations in the size of the turbulent structures in the circumferential direction.

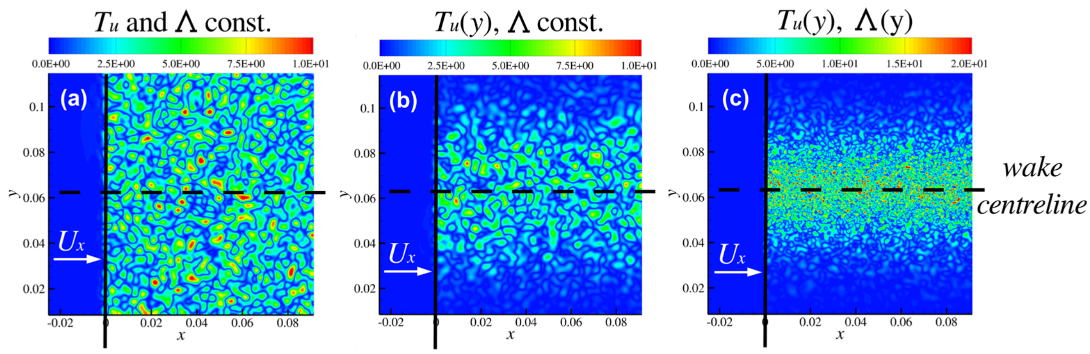

Figure 7. Contours of non-dimensional vorticity magnitude ($\|\nabla \times \boldsymbol{u}\| L_{ref}/c_0$) using different fan wake modelling assumptions

The numerical implementation is validated by comparison of analytical and numerical one-dimensional spectra averaged in the circumferential direction, as shown in Fig. 8. A good agreement is found at all frequencies for the different fan wake modelling assumptions examined.

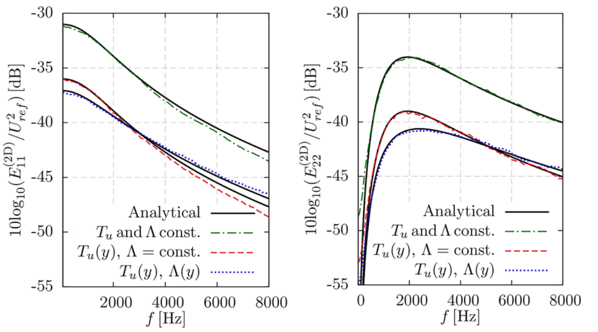

Figure 8. Von Kármán one-dimensional spectrum of streamwise (left) and transverse (right) fluctuating velocity averaged in the circumferential direction

5. INFLUENCE OF FAN WAKE MODELLING ON BROADBAND NOISE

In this section, the fan wake modelling assumptions presented and validated in Section 4 are tested for broadband noise predictions of turbulence-cascade interaction.

5.1 Computational Setup

A schematic of the CAA domain is shown in Fig. 9. Throughout this study, the chord of the OGVs is fixed to $c = 0.15$ m, the stagger angle is set to $\alpha = 0°$, and the gap-to-chord ratio is $s/c = 0.75$.

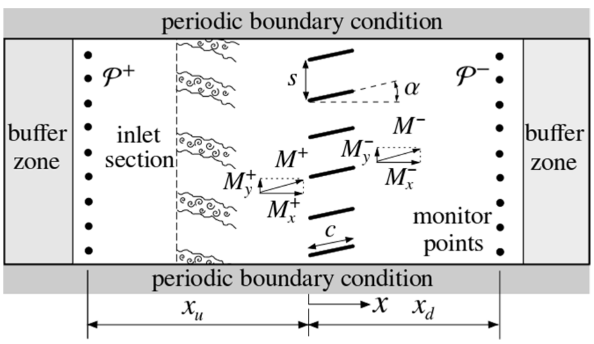

Figure 9. Computational setup for simulations of turbulence-cascade interaction noise

Arrays of 225 monitor points that are uniformly distributed in the circumferential direction are placed upstream, $x_u = -1.5c$, and downstream of the cascade, $x_d = 2.5c$, to collect samples of fluctuating pressure. These arrays of monitor points were located far enough from the cascade to ensure that only cut-on modes contribute to the sound power spectra, which can be computed as

$$\mathcal{P}^{\pm}(\omega) = \frac{Bs}{\rho_0}\mathrm{Re}\left\{\sum_{l=-\infty}^{+\infty}|\hat{p}_l(\omega)|^2 \frac{\omega}{\left|\omega+U_x^{\pm}k_{x,l}^{\pm}+U_y^{\pm}k_{y,l}\right|^2}\left[-k_{x,l}^{\pm *}+\frac{U_x^{\pm}}{c_0^2}\left(\omega+U_x^{\pm}k_{x,l}^{\pm}+U_y^{\pm}k_{y,l}\right)\right]\right\}, \qquad (11)$$

where the superscript '+' denotes upstream and '-' denotes downstream, ()* represents the complex conjugate, $\mathrm{Re}\{.\}$ is the real part operator, B is the number of vanes, $\omega = 2\pi f$ corresponds to the angular frequency, $\hat{p}_l(\omega)$ is the amplitude of the fluctuating pressure from a spatio-temporal Fourier transform, $k_{y,l} = 2\pi l/(Bs)$ is the acoustic wavenumber in the circumferential direction, l is an integer number that represents the order of the acoustic mode in the circumferential direction, and the acoustic wavenumber in the axial direction is given by

$$k_{x,l}^{\pm} = \frac{M_x^{\pm}\left(\frac{\omega}{c_0}+M_y^{\pm}k_{y,l}\right)\pm\sqrt{\left(\frac{\omega}{c_0}+M_y^{\pm}k_{y,l}\right)^2-\left[1-\left(M_x^{\pm}\right)^2\right]k_{y,l}^2}}{1-\left(M_x^{\pm}\right)^2}. \qquad (12)$$

All numerical simulations of turbulence-cascade interaction noise were run by using the von Kármán spectrum in Eq. 1 with $T_u = 0.017$, $\Lambda = 0.008$ m to define the spectral content of the fan wakes, as detailed in Section 4.4.2.

Note that the absence of the fan stage in the CAA simulations prevents potential shielding effects on upstream-travelling pressure waves from being taken into account in the sound power spectra.

5.2 Effects of fan wake modelling on noise

A cascade of NACA 0001 aerofoils with *B=4* in a uniform mean flow at $M = 0.6$ is used to assess potential effects of fan wake modelling on turbulence-cascade interaction noise. When modelling cyclostationary variations in the statistics of the fan wakes, $n_w = 4$, and $\Omega = 2640$ rad/s.

Fig. 10 shows instantaneous contours of non-dimensional fluctuating vorticity magnitude and fluctuating pressure in the simulation with variations in the turbulence intensity $(T_u(y), \Lambda =$

const.). The effectiveness of the periodic boundary condition in the circumferential direction can be observed in the fluctuating pressure contours, which also show a number of cut-on modes propagating upstream and downstream of the cascade.

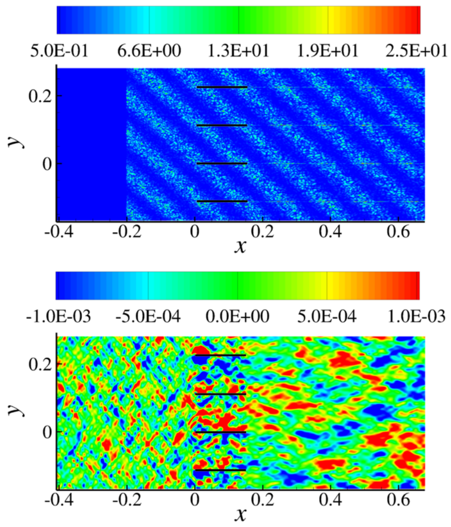

Figure 10. Contours of non-dimensional vorticity magnitude ($\|\nabla \times \boldsymbol{u}\| L_{ref}/c_0$) and fluctuating pressure ($p'/(\rho_0 c_0^2)$)

Numerical sound power spectra are compared to analytical predictions using Cheong *et al.*'s flat plate model for two-dimensional cascades [26]. The analytical predictions were obtained by using the circumferentially-averaged transverse velocity spectrum, so that the fan wake modelling is not included in the analytical model.

Fig. 11 shows the PWL spectra radiated by the cascade of NACA 0001 aerofoils. A good agreement is found between the analytical predictions and the CAA results, which suggests that broadband noise mainly relies on the averaged spectrum that is perceived by the cascade, and not in the instantaneous statistics of the fan wake.

Consequently, a more realistic description of the fan wake, with its associated increase in complexity and computational cost, does not necessarily correspond to a more accurate broadband noise prediction, at least when $\Lambda \ll c$. This result reinforces the idea of using isotropic turbulence to fit a circumferentially-averaged spectrum of the fan wakes for OGV noise predictions.

When comparing Figs. 11(a) and 11 (b), it can also be observed that cyclostationary variations in the turbulence intensity ($T_u(y), \Lambda = \text{const.}$) do not affect the shape but the amplitude of the spectra in comparison with isotropic turbulence (T_u and Λ const.). Particularly, the noise spectra are scaled by $4.4\,\text{dB}$, which corresponds to $10\log_{10}(A_{w,rms}^2)$. Thus, if the integral length scale is assumed to be constant, cyclostationary variations in the turbulent kinetic energy can only scale the sound power spectrum. This finding is consistent with previous works in the field [12, 14, 17].

When including cyclostationary variations in the integral length scale for the fan wake modelling, the energy is slightly redistributed over the whole frequency range, affecting the slope of the sound power spectra. Thus, Fig. 11(c) shows a slight decay in the noise levels (~2dB) for $fc/U < 4$ but similar noise levels for $fc/U > 5$ in comparison with Fig. 11(b). These trends in the shape of the spectrum are closely related to the variations experienced by the transverse one-dimensional spectrum averaged in the circumferential direction, as shown in Fig. 8. Also, similar effects were reported by *Ju et al.* [17] when using different values of the integral length scale for background and wake turbulence.

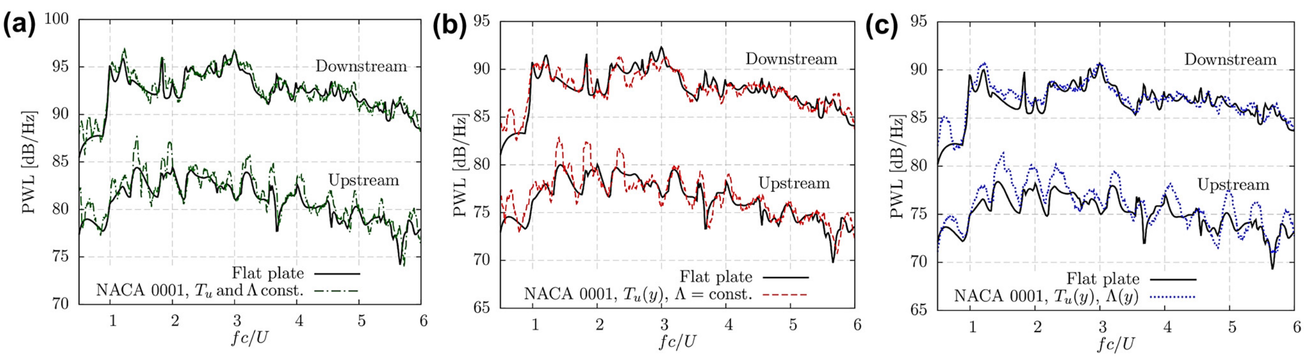

Figure 11. PWL spectra from a cascade of NACA 0001 aerofoils for different fan wake modelling assumptions

6. PARAMETER STUDY ON CASCADE NOISE USING ISOTROPIC TURBULENCE

This section extends the parameter study on turbulence-cascade interaction noise presented by Gea-Aguilera *et al.* [6], in which the effects of mean flow Mach number, aerofoil thickness, stagger angle, and s/c ratio on broadband noise were assessed. Here, the effects of vane count and camber are investigated by using aerofoils with 6% and 12% thickness relative to the chord. All simulations in this section are performed with $s/c = 0.75$ and $\alpha = 0°$. A steady and inviscid mean flow is used for the CAA simulations, since viscosity effects have been shown to play a negligible role on leading edge noise predictions, and a uniform mean flow cannot account for the distortion of the turbulent structures in the leading edge region [15]. The mean flow Mach number is set to 0.3 upstream of the cascade.

Isotropic synthetic turbulence, as detailed in Section 4.1, is used to reproduce the two-dimensional von Kármán spectrum defined in Eq. 1 with $T_u = 0.017$, $\Lambda = 0.008$ m.

6.1 Vane count effect on noise

Broadband noise predictions of turbulence-cascade interaction normally require the inclusion of a full annulus in order to account for refraction effects and the correct cut-on acoustic modes that can propagate in the duct. However, single OGV passages have been used in previous numerical studies to reduce the size of the mesh, and therefore the computational expense [5, 10].

In this section, cascades of NACA 0012 aerofoils with 1, 4, and 20 vanes are simulated in the CAA solver to assess the effect of vane count on noise. Figs. 12 and 13 show PWL spectra per vane upstream and downstream of the cascade, respectively. Noise predictions from CAA simulations were compared with Cheong *et al.*'s flat plate model [26]. Results show a significant noise reduction due to aerofoil thickness at high frequencies, which is consistent with previous works of single aerofoils in the freestream [15,16].

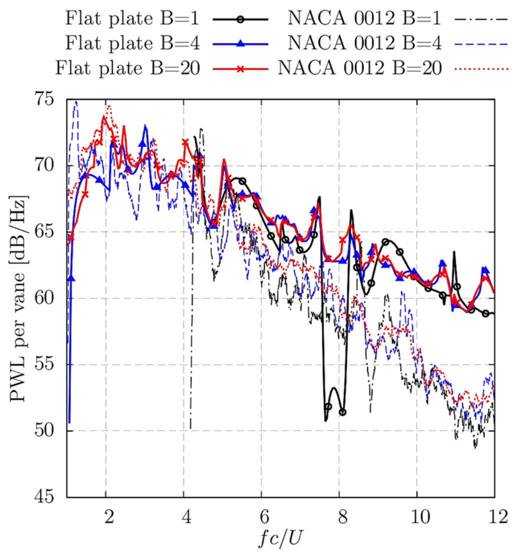

Figure 12. Upstream PWL spectra for different vane counts

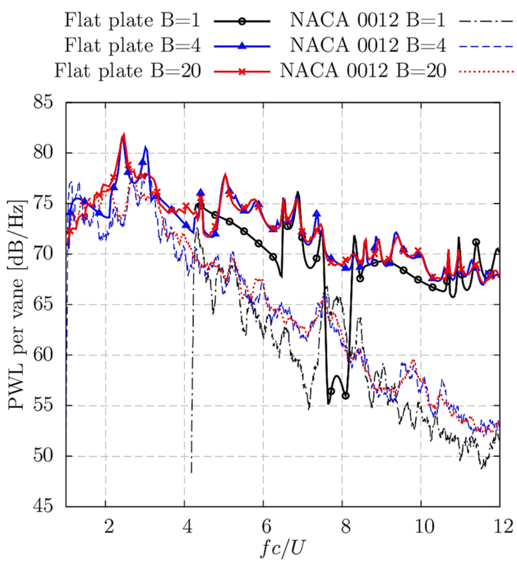

Figure 13. Downstream PWL spectra for different vane counts

Simulations with a single vane passage cannot give accurate noise predictions for low frequencies due to the small width of the CAA domain, which limits the cut-on modes that can propagate. Based on Cheong *et al.*'s analytical model [26], the minimum frequency that can propagate for a zero stagger angle flat plate is

$$f_{min} = \frac{c_0\sqrt{1-M_1^2}}{Bs}, \qquad (13)$$

which corresponds to $fc/U = 4.2$ for the cascade simulation with $B = 1$, as shown in Figs. 12 and 13. Paruchuri *et al.* [9] highlighted that the reduced frequency range of interest for fan broadband noise applications is around $fc/U = 2$, which corresponds to the third harmonic of the blade passing frequency of a conventional turbofan engine at approach conditions. Thus, at least $B = 4$ vanes should be used to cover the reduced frequency range of interest. However, significant discrepancies (of up to $4\ \mathrm{dB}$) can be found in PWL spectra at low frequencies ($fc/U < 4$). This highlights the importance of taking into account the total number of vanes for correct broadband noise predictions in the frequency range of interest for fan noise applications.

At high frequencies, there is a good collapse in the shape and noise levels of the sound power spectra per vane, especially for $B \geq 4$. Thus, it is possible to reduce the number of vanes computed when investigating high frequencies, since PWL spectra increase with the number of vanes at high frequencies as $10\log_{10}(B)$. Therefore, thick aerofoils seem to behave as uncorrelated noise sources at high frequencies, as found in previous studies for flat plates [26, 27].

6.2 Camber effects on noise

This section studies the effects of camber on turbulence-cascade interaction noise. Using a symmetric NACA 0006 aerofoil cascade with $B = 4$ as a baseline case, the camber is increased up to 6% of the aerofoil chord.

The majority of analytical models for cascade noise assume a constant stagger angle and unloaded flat plates, and therefore, the direction of the mean flow remains the same on both sides of the cascade. In contrast, Eq. 11 can account for variations in the mean flow direction across the cascade to compute sound power spectra from the CAA simulations. This is particularly relevant when dealing with cambered aerofoils, which may vary the direction of the mean flow, adding or removing swirl.

The mean flow used in the CAA simulations is significantly affected by the camber, as shown in Fig. 14 for the NACA 0006 and NACA 6406 aerofoil cascades. Although the stagger angle is kept to zero, the camber induces a change in the direction of the mean flow downstream of the cascade, and a shift in the stagnation region towards the suction side, which varies the angle of attack that is perceived by the aerofoils.

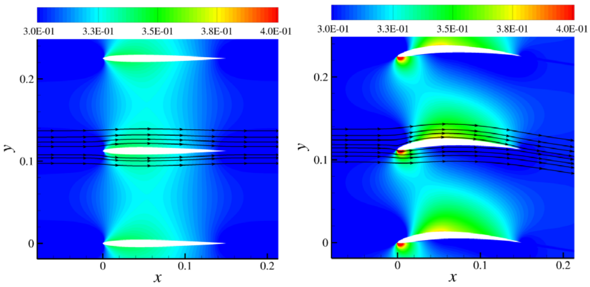

Figure 14. Contours of Mach number around a cascade of NACA 0006 (left) and NACA 6406 (right) aerofoils

PWL spectra upstream and downstream of the cascade are shown in Figs. 15 and 16, respectively. Despite the significant change in the mean flow distribution around the cascade, there is a good overlap in PWL spectra for different degrees of camber, which suggest a small effect of camber on the overall noise. For the 6% camber aerofoil, a consistent increase in upstream PWL of only 1 dB is found at the majority of frequencies with respect to low-cambered aerofoils. These findings agree with previous works by Paruchuri *et al.* [9], and Evers and Peake [28], in which variations in the total radiated power within $1 - 2\ \mathrm{dB}$ were reported for cambered aerofoil cascades.

It can also be observed that noise reduction at high frequencies due to aerofoil thickness is significantly smaller for NACA 0006 aerofoils than for NACA 0012 aerofoils (see Figs. 12 and 13). Thus, thin aerofoils present PWL spectra that resembles those of flat plate predictions over a large portion of the frequency spectrum. This result reinforces the validity of the flat plate assumption for OGV noise predictions.

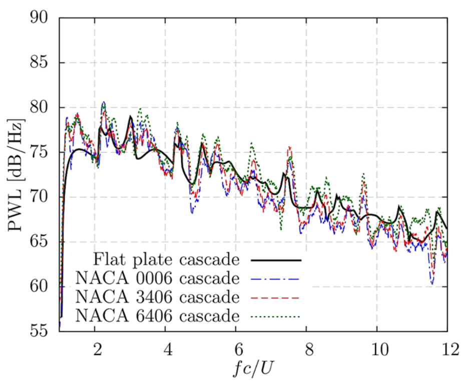

Figure 15. Upstream PWL spectra for different cambered aerofoils

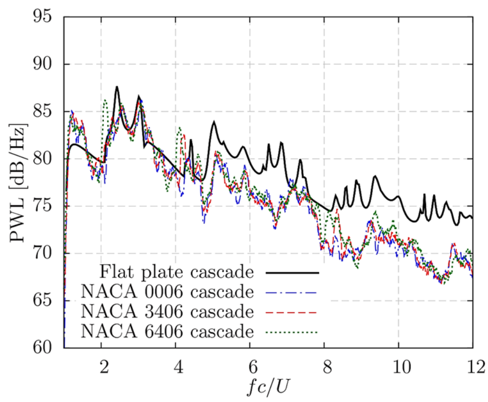

Figure 16. Downstream PWL spectra for different cambered aerofoils

7. CONCLUSIONS

A synthetic turbulence method based on digital filters has been presented and validated to reproduce the statistics in the fan wakes. Three different fan wake modelling assumptions have been proposed: (a) isotropic turbulence, (b) cyclostationary variations in turbulent kinetic energy with a constant integral length scale, and (c) cyclostationary variations in both turbulent kinetic energy and integral length scale. These assumptions have been used in CAA simulations of turbulence-cascade interaction noise. PWL spectra show that broadband noise mainly depends on the circumferentially-averaged turbulence spectra that interact with the cascade. A realistic description of the fan wake, with spatio-temporal variations in both turbulent kinetic energy and integral length scale, does not lead to a significant improvement of broadband noise prediction. Thus, the isotropic turbulence assumption provides the best compromise between computational cost and simulation accuracy.

When using a single passage vane in CAA simulations to study cascade noise, the minimum frequency that can be solved due to the width of the CAA domain is normally larger than the frequency range of interest for fan broadband noise applications. By increasing the vane count, PWL spectra per unit vane overlap at high frequencies, but there are still some discrepancies in the shape of the spectrum at low frequencies, which suggest the need for the total vane count for high-fidelity noise predictions.

Camber effects on cascade noise have been studied on 4-digit NACA aerofoils with 6% maximum thickness-to-chord ratio, which is representative of a typical OGV thickness in modern turbofan engines. PWL spectra show a negligible effect of camber on the noise levels ($\sim 1\,\mathrm{dB}$), despite the significant variation that camber causes in the mean flow. Also, PWL spectra from 6% thickness aerofoils match satisfactorily the analytical flat plate results over a large portion of the frequency range, before aerofoil thickness effects on noise become evident, which reinforces the use of the flat plate assumption for the prediction of OGV cascade noise.

8. REFERENCES

1. European Commission (2011). Report of the High Level Group on Aviation, Flightpath 2050 Europe's Vision for Aviation.
2. Ganz, U.W., Joppa, P.D., Patten, T.J. & Scharpf, D.F. (1998). Boeing 18-Inch Fan Rig Broadband Noise Test. NASA Contractor Report CR-1998-208704.
3. Casalino, D., Hazir, A. & Mann, A. (2016). Turbofan Broadband Noise Prediction Using the Lattice Boltzmann Method. In Proc. 22nd AIAA/CEAS Aeroacoustics Conference, No. AIAA 2016-2945, Lyon, France.
4. Casalino, D. & Hazir, A. (2016). Lattice Boltzmann Based Aeroacoustic Simulation of Turbofan Noise Installation Effects. In Proc. 23rd International Congress on Sound and Vibration, Athens, Greece.
5. Greschner, B. & Thiele, F. (2012). Broadband Noise Analysis of a Rotor-Stator-Cascade Using Wall Modeled LES Simulation. In Proc. 18th AIAA/CEAS Aeroacoustics Conference, No. AIAA 2012-2308, Colorado, Springs.
6. Gea-Aguilera, F., Gill, J., Zhang, X. & Nodé-Langlois, T. (2016). Turbulence-Cascade Interaction Noise Using an Advanced Digital Filter Method, In Proc. 23rd International Congress on Sound and Vibration, Athens, Greece.
7. Envia, E. (2004). Fourth Computational Aeroacoustics (CAA) Workshop on Benchmark Problems - Category 3 - Problem 2 - Cascade-Gust Interaction. NASA Conference Publication CP-2004-212954.
8. Namba, M. & Schulten, J.B.H.M. (2000). Third Computational Aeroacoustics (CAA) Workshop on Benchmark Problems - Category

4 - Fan Stator with Harmonic Excitation by Rotor Wake. NASA Conference Publication CP-2000-209790.
9. Paruchuri, C., Coupland, J. & Joseph, P. (2016). Airfoil Geometry Effects on Broadband Interaction Noise in Cascades. In Proc. 22nd AIAA/CEAS Aeroacoustics Conference, No. AIAA 2016-2738, Lyon, France.
10. Polacsek, C., Clair, V., Le Garrec, T., Reboul, G. & Jacob, M.C. (2015). Numerical Predictions of Turbulence/ Cascade-Interaction Noise Using Computational Aeroacoustics with a Stochastic Model. *AIAA Journal*, **53**(12), 3551-3566.
11. Ewert, R. (2008). Broadband Slat Noise Prediction based on CAA and Stochastic Sound Sources from a Fast Random Particle-Mesh (RPM) Method. *Journal of Computers and Fluids*, **37**(4), 369-387.
12. Dieste, M. (2011). Random-Vortex-Particle Methods Applied to Broadband Fan Interaction Noise. Thesis for the degree of Doctor of Philosophy, ISVR, University of Southampton.
13. Jurdic, V., Joseph, P. & Antoni, J. (2009). Investigation of Rotor Wake Turbulence Through Cyclostationary Spectral Analysis. *AIAA Journal*, **47**(9), 2022-2030.
14. Wohlbrandt, A. M., Guérin, S. & Ewert, R. (2015). Extension of the Random Particle Mesh Method to Periodic Turbulent Flows for Fan Broadband Noise Prediction. In Proc. 21st AIAA/CEAS Aeroacoustics Conference, No. AIAA 2015-2383, Dallas, Texas.
15. Gill, J., Zhang, X. & Joseph, P. (2013). Symmetric Airfoil Geometry Effects on Leading Edge Noise. *Journal of the Acoustical Society of America*, **134**(4), 2669-2680.
16. Paruchuri, C., Gill, J., Narayanan, S., Joseph, P., Vanderwel, C., Zhang, X. & Ganapathisubramani, B. (2015). Aerofoil Geometry Effects on Turbulence Interaction Noise. In Proc. 21st AIAA/CEAS Aeroacoustics Conference, No. AIAA 2015-2830, Dallas, Texas.
17. Ju, H., Mani, R., Vysohlid, M. & Sharma, A. (2015). Investigation of Fan-Wake/Outlet-Guide-Vane Interaction Broadband Noise. *AIAA Journal*, **53**(12), 3534-3550.
18. Gea-Aguilera, F., Zhang, X., Chen, X., Gill, J. & Nodé-Langlois, T. (2015). Synthetic Turbulence Methods for Leading Edge Noise Predictions. In Proc. 21st AIAA/CEAS Aeroacoustics Conference, No. AIAA 2015-2670, Dallas, Texas.
19. Gea-Aguilera, F., Gill, J., Zhang, X., Chen, X. & Nodé-Langlois, T. (2016). Leading Edge Noise Predictions Using Anisotropic Synthetic Turbulence. In Proc. 22nd AIAA/CEAS Aeroacoustics Conference, No. AIAA 2016-2840, Lyon, France.
20. Jarrin, N., Benhamadouche, S., Laurence, D. & Prosser, R. (2006). A Synthetic-Eddy-Method for generating Inflow Conditions for Large-Eddy Simulations. *International Journal of Heat and Fluid Flow*, **27** (4), 585-593.
21. Sescu, A. & Hixon, R. (2013). Towards Low-Noise Synthetic Turbulent Inflow Conditions for Aeroacoustic Calculations. *International Journal for Numerical Methods in Fluids*, **73** (12), 1001-1010.
22. Nallasamy, M. & Envia, E. (2005). Computation of Rotor Wake Turbulence Noise. *Journal of Sound and Vibration*, **282**, 649-678.
23. Maunus, J., Grace, S., Sondak, D. & Yakhot, V. (2013). Characteristics of Turbulence in a Turbofan Stage. *Journal of Turbomachinery*, **135**(2), 021024.
24. Kraichnan, R. (1970). Diffusion by a Random Velocity Field. *The Physics of Fluids*, **13**(1), 22-31.
25. Pope, S. (2000). Turbulent flows. *Cambridge University Press*, UK.
26. Cheong, C., Joseph, P. & Lee, S. (2006). High Frequency Formulation for the Acoustic Power Spectrum due to Cascade-Turbulence Interaction. *Journal of the Acoustical Society of America*, **119**(1), 108-122.
27. Blandeau, V. P., Joseph, P. F., Jenkins, G., & Powles, C. J. (2011). Comparison of Sound Power Radiation from Isolated Airfoils and Cascades in a Turbulent Flow. *Journal of the Acoustical Society of America*, **129**(6), 3521-3530.
28. Evers, I. & Peake, N. (2002). On sound generation by the interaction between turbulence and a cascade of airfoils with non-uniform mean flow. *Journal of Fluid Mechanics*, **463**, pp. 25-52.